Journal of Hydrology (NZ) 50 (2): 339-360 2011

A mobile rain radar for high resolution hydrological observations in New Zealand

Luke Sutherland-Stacey, Paul Shucksmith and Geoff Austin

Atmospheric Physics Group, University of Auckland, Private Bag 92019, Auckland, New Zealand. Corresponding author: l.sutherland-stacey@auckland.ac.nz

Abstract

Rain processes operate at a wide range of spatial and temporal scales, and significant variability in precipitation occurs over physical extents and timeframes that are poorly sampled by operational observing systems, even by the comparatively fine sampling capabilities of national radar networks. At present, measurements with the highest spatial and temporal resolution are made with research radars. This paper describes an X-band mobile weather radar system that has been constructed at the University of Auckland, New Zealand, to make observations with high spatial (≈100 m) and temporal (≈15 sec) resolution. A description of some recent field work is presented, with particular attention to sampling scale problems. The radar was deployed overlooking a small (≈150 km^2), steep, catchment in the central North Island of New Zealand during the winters of 2008 and 2009. Data from the field work is used to qualitatively demonstrate the need for high resolution measurements for rigorous observation of small-scale structures such as discrete convective cells and larger systems with embedded convection. The sampling representivity errors associated with such meteorological systems are discussed for X- and C-band radars. X-band radar rainfall rate retrievals are also compared to a gauge network. Statistical analysis of the comparison for short ranges (<15 km) gave RMS error statistics of c. 1 mm/hr, but agreement was poorer at longer ranges (>15 km) due to site limitations and to low radar power and attenuation limitations. The implications of the scale limitations of conventional measurement techniques for sampling rainfall accumulation over small catchments are also discussed, with an illustrative example from the field work.

Introduction

The use of weather radar in the fields of meteorology and hydrology is well established. Many countries around the world operate national radar networks, usually consisting of large C-band or S-band radar systems designed for maximum coverage or versatility (Cheze, 2002; Crum and Alberty, 1993). The New Zealand Meteorological Service (NZ MetService) runs a number of Dopplerised C-band radars, seven at the date of publication, with two additional radars due for installation by the end of 2013 (for an early overview of the New Zealand national radar network, see Crouch, 2003). National radar networks observe large-scale precipitation at range-dependent resolutions varying between hundreds of metres and a few kilometres in space and several minutes in time. This resolution is sufficient to characterise the overall distribution and intensity of precipitation; however it is evident that precipitation processes at scales much

less than those captured by existing networks are present within the larger rain structures (Fiener and Auerswald, 2009; Pedersen *et al.*, 2010).

The spatial coverage of weather radar networks is inevitably more complete than that of rain gauge networks. Rain gauges measure accumulations only at particular points in space, and gauges only a few kilometres apart may show significant variability in rainfall (Bitew and Gebremichael, 2010; Changnon, 2002), leading to significant uncertainty in rain gauge based areal accumulation estimates (Villarini *et al.*, 2008). This has important implications when using rain gauge data as input for hydrological models, as errors in spatial and temporal areal rainfall estimates may result in large errors in model response (Krajewski *et al.*, 1991; Cho *et al.*, 2009; Cooper and Fernando, 2009; Duncan *et al.*, 1993). The origin of this uncertainty is related to the fact that rain structure may vary on scales much shorter than gauge spacing – rain systems capable of delivering significant accumulation can either fit between gauges and go unobserved or fall on a gauge but not occur elsewhere where no observations are made. As radar observations are spatially contiguous, radar-derived precipitation fields are often used to supplement, or indeed replace, direct in-situ rain-gauge measurements for a variety of scientific and hydrological engineering applications. These include catchment modelling and flood forecasting (Delrieu *et al.*, 2009; Reichel *et al.*, 2009), as well as the provision of data for improving short-term numerical weather forecasts (e.g., Xiao *et al.*, 2007) or nowcasts of precipitation (e.g., Larsen and Gray, 2003).

For this paper we assume the reader is largely familiar with the basic principles of radar meteorology. A complete review of radar theory may be found in any radar meteorology textbook (e.g., Doviak and Zrnic, 1993). As a reminder, precipitation rate (R) at the surface is inferred from radar reflectivity (Z) measurements made aloft through empirical "Z-R" relationships based on assumptions about the average drop-size distribution of rain (after Marshall and Palmer, 1948). It is well known that there are numerous potential sources of error associated with the retrieval of surface rainfall rate; including errors stemming from variability in drop-size distribution, beam spreading and overshooting of meteorological targets and the variability of hydrometeor class with height (for a review see Villarini and Krajewski (2010)).

Much effort has been expended investigating uncertainties related to the parameterisation of drop-size distributions and the resulting impact on Z-R relationships, and the error introduced when propagating information made from measurements aloft to the surface (Gray, Uddstrom and Larsen, 2002). It is difficult to infer surface rainfall rate from radar measurements taken (necessarily) high above the ground, as there is significant uncertainty as to the extent to which measurements made aloft are representative of the surface accumulation.

In the case of cool large-scale condensation processes (or stratiform rain), additional uncertainty is introduced by the variations in hydrometeor class with altitude. Snow and ice have a comparatively weak radar reflectivity compared to liquid water (due to a lower dielectric factor), but, if falling to warmer layers, they begin to melt and temporarily acquire a liquid water coating. The resulting 'wet' solid particle is less dense than liquid water but reflects as a rain droplet, contributing significantly to radar reflectivity. As the low-density particle melts, its density increases while its size decreases, thus increasing its terminal velocity. The increase in terminal velocity spreads out individual hydrometeors in the vertical, reducing the density of hydrometeors in the beam cross-section, so that the reflectivity is then once

again decreased. This phenomenon, described by Austin and Bemis (1950), following Ryde (1946) and Cunningham (1947), results in an enhanced reflectivity signal, or bright band, at the melting layer (just below the zero degree isotherm), and introduces difficulties when applying a Z-R relationship to measurements made in or above this region. If a reflectivity measurement is made far enough below the bright band, then the observation should be sufficiently representative of the surface to allow rainfall rate determination. Convective cells usually exhibit a complex reflectivity structure, and if they are deep enough, with strong enough updraft cores, they often involve the formation of frozen hydrometeor classes, which further complicates the application of the Z-R relationship to retrieve surface rainfall rate.

While these sources of error have been extensively explored over the last 60 years, less attention has been paid to the fundamental sampling errors associated with measuring precipitation using observation sampling intervals and spatial resolutions that are coarse compared with precipitation systems' de-correlation length and time. Fabry *et al.* (1994) demonstrated that, for a small data set, the spatial and temporal sampling errors associated with radar accumulation retrievals may make up the largest source of uncertainty at kilometre resolutions on short time scales.

Little attention is paid to this error source with respect to radar observations as little can be done to improve the spatial sampling of existing fixed radar networks without increasing the density of the network or changing the fundamental parameters of the radars.

One improvement, increasing the down-range resolution of the radar, can nowadays be easily implemented with software and minor upgrades. The NZ MetService completed such an upgrade in 2006, reducing the radial resolution from 2 km to 125 m. Azimuth de-convolution to sharpen the image is possible but more technically difficult to implement (Austin, 1974).

The primary limit on radar axial resolution is the distance from the radar to the observed hydrometeors and the angular width of the antenna beam. For example, the various New Zealand national C-band radars have beam widths of 0.86, 0.95 or 1.65 degrees (there is some variability in dish dimensions and operating wavelengths between different generations of radars within the network). For the narrowest beam width this translates into a beam cross-section of 150 m at 10 km, 1.5 km at 100 km and 3.75 km at the maximum range of 250 km. At longer ranges it is self-evident that variations in target density in the vertical and azimuthal direction cannot be adequately resolved with a beam of modest width, although some useful qualitative information will still be obtained. When using weather radar for hydrology, this means that although information may be available out to the radar's maximum range, it may not be representative of rainfall rate and therefore not useful for quantitative hydrology.

A natural solution to the spatial resolution problem therefore is to move the radar closer to the study site. Although this solution is clearly impractical in the case of the large fixed-location C or S-band radars typical of national networks, a number of university research groups run mobile rain radars mounted on a variety of vehicles (e.g., Biggerstaff *et al.*, 2005; Bluestein *et al.*, 2007; Wurman *et al.*, 1997), which permit the radars to be stationed as near as possible to regions of interest, and in some cases even record data while moving. The University of Auckland Atmospheric Physics Group (UoAAPG) has also operated several mobile rain radars in recent years. UoAAPG radars have been mounted on an eclectic fleet of vehicles, including a van, a caravan and a 1/4-sized shipping container. These radars have participated in a number of large field campaigns, including the Southern Alps Experiment (SALPEX, Purdy *et al.*,

2005) and the Mahurangi River Variability Experiment (MARVEX, Woods *et al.*, 2001). Smaller field campaigns have also made interesting observations of relatively rare natural phenomena such as the 1996 volcanic eruption at Mt Ruapehu (Mann, 1998) and a tornado near Auckland (Sutherland-Stacey, Shucksmith and Austin, 2010).

Temporal resolution limitations can be minimised by scanning more quickly (increasing the rotational velocity of the radar dish) or reducing the number of different dish elevations used to make up a scan cycle. Once again, national radar networks tend to be limited in this regard by operational requirements. For example, comprehensive volume scans including higher elevations may be required for aviation, and increasing the dish rotational velocity may not be possible if a slow Doppler scan is incorporated in the observation cycle. In the future it is likely that the frequency of scan cycles will be greatly improved by the adoption of phased array technology (in which the radar beam is steered electronically, not mechanically). However, it will be some time before civilian phased-array radars are not prohibitively expensive, and at present the experimental versions have larger beam widths than their mechanically steered counterparts (Collier *et al.*, 2011; Heinselman and Torres, 2011). In the meantime, small conventional research radars have the flexibility to operate at high scan rates.

High resolution radar observations from mobile radar are well suited for detailed characterisation of rainfall types and distribution, as they allow the vertical and horizontal variability of rain fields to be resolved. In particular, orographic rain, in which atmospheric flow deflected up and over terrain may trigger new rain or enhance existing precipitation upwind of the obstruction to the detriment of rainfall downwind, can result in very high and localised rain rates. Orographic rainfall delivers significant precipitation along the western slopes of the Southern Alps of New Zealand (Henderson and Thompson, 1999) but is not well observed by the existing fixed radar network. The nearby national C-band radars are located on the more densely populated eastern side of the South Island and cannot image low-altitude precipitation on the other side of the central mountain range. Small X-band radars are ideally suited for the study of orographic processes, as they may be sited close enough to steep catchments to avoid beam blocking from terrain and image the low-altitude orographic rain that is often unobserved by more distant fixed radars (Gray and Seed, 2000). These small radars can scan with high enough spatial and temporal resolution to resolve the rapidly evolving system for microphysical interpretation (Purdy *et al.*, 2005; Prat and Barros; 2010). A variety of precipitation processes, for example, the microphysics of melting hydrometeors and corrections for bright band effects (Fabry and Zawadzki, 1995), can be analysed using X-band radar observations.

For hydrological applications modelling small steep catchments, it is advantageous to have high resolution radar observations of rain fields, due to the complex behaviours of these hydrological systems with uncertain distributions of rainfall (McMillan *et al.*, 2011). The path which an individual convective cell tracks across a small catchment may have a vastly different impact on catchment outflow than equivalent rainfall delivered by widespread stratiform rain, but, as discussed later, may be difficult to resolve with conventional gauge or national radar observations.

This paper describes a new mobile radar which has recently been designed and constructed by the UoAAPG and provides an example of the spatially and temporally resolved precipitation data relevant to hydrology that can be collected. The radar

was recently employed for a case study of a small catchment, which is described, along with radar-gauge calibration results and a discussion of the implications for hydrological modelling of rain field data with a high spatial and temporal resolution.

The University of Auckland Trailer Radar

The UoAAPG Trailer Radar consists of a fully articulated dish mounted on a short tower, coupled by flexible waveguide to a masthead transceiver; the outputs are in turn fed, along with information regarding the dish direction, into a personal computer housed in a small operator's cab. The entire system is powered by either a 4 kW diesel generator or by two single-phase mains connections.

The radar system is entirely self-contained on a tandem axle trailer. The total mass is about 2.5 tonnes, allowing it to be towed by a light four-wheel-drive vehicle; provided that the trailer's hydraulic breaking system is used. The radar mast is folded down onto the trailer for transport. On arrival at a field site, the mast can be erected and the radar made ready by a team of two. An image of the new radar is shown in Figure 1.

Figure 1 – The Trailer Radar deployed at the field site overlooking the Waipapa catchment.

The radar transceiver is a Decca Bridgemaster X-band (3.2 cm) pulsed 25 kW non-Doppler marine radar. The transceiver is not significantly modified from off-the-shelf specifications, although small changes have been made with the manufacturer's assistance to allow operation without the use of the standard marine antenna, motor assembly and control unit. The transceiver is coupled to a 1.2 m parabolic dish through a customised flexible waveguide and feed. A 1.8 degree beam width is realised with this assembly (calculated after Doviak and Zrnic, 1993, p. 34, eqs. 3.2a and 3.2b). The choice of an X-band transceiver instead of a C-band (≈5 cm) transceiver is a pragmatic one. C-band radiation is weakly attenuated by liquid water compared to X-band systems, improving the quality of reflectivity measurements at range, however, a larger dish is required to realise an equivalent beam width with a C-band system. A difference between X-band and C-band transceivers is also apparent from the denominator in the radar reflectivity equation (Doviak and Zrnic, 1993, eqs. 3.6 and 3.24) – the shorter the wavelength the higher the sensitivity for radars with the same transmitting power. For a mobile radar, increasing dish size and transceiver power has significant engineering and cost consequences. As the major design brief was for short-range operation and a portable system, an X-band transceiver was preferable.

The dish is steered with low-speed DC motors, giving turning rates of 20 deg s^{-1} in elevation and 36 deg s^{-1} in azimuth. A notable feature of the assembly is a military-surplus tank turret bearing used to support the azimuthal pivot. The range of motion of the dish is from 0° to 100° in elevation and from -270° to +270° in azimuth. Drive encoders provide 12 bit directional resolution in each axis. Because of the cabling geometry, the dish scans clockwise and then anticlockwise in

azimuth, not continuously in one direction as other radars commonly do.

Dish orientation and the reflectivity signal are digitised at a resolution selected by the user, using a personal computer running Linux. The computer incorporates a high-speed PCI Analog to Digital Converter (Exacq CH-3150) and a Digital I/O card (Sealevel Systems 8005). The radar software has been programmed in C, C++ and MATLAB (2007b, The Mathworks, Natick, Massachusetts, USA) by graduate students and uses the open source Real Time Application Interface (RTAI, Dozio and Mantegazza, 2003) to synchronise recording of the dish position and the radar return signal, as well as the dispatch of instructions to the drive motors.

The control system also incorporates wind speed input. If high wind speeds (running average greater than 30 ms^{-1}) are detected, the dish is parked pointing vertically to present a minimum cross-section, thus protecting itself from possible damage.

During normal operation, the radial reflectivity data is averaged over a pre-set number of pulses and then stored, along with dish direction information, in a raw binary format for later processing and analysis. To account for the well known attenuation problems associated with X-band radar observations, in which the return from distant scatterers may be significantly reduced or even completely obscured by those closer to the radar (Ryde, 1946; Atlas and Banks, 1951) the data optionally can be corrected for attenuation using an iterative method that estimates the attenuation at each range bin (Nicol and Austin, 2003). Similar attenuation correction has been shown in a number of studies to improve precipitation retrievals (van de Beek *et al.*, 2010). Finally the data is transformed into Cartesian coordinates – as the range of the radar is short (at most 50 km) a flat earth approximation is used.

Further optional on-the-fly processing of the Cartesian data includes removal of, or interpolation over, reflectivity returns contaminated with ground clutter. After ground-clutter treatment, images can be fed into a rapid-update nowcast to diagnose the echo motion and adjust an optional vertical cross-section scan task to point upwind. The Cartesian data is then zero compressed for storage and can be streamed offsite via an internet link and an image is automatically generated for dissemination via a campus web server. The personal computer, non-weathertight electronics and graduate students are housed in an air-conditioned cab at the back of the trailer.

The power requirements of the entire radar system are less than 2 kW under normal operating conditions. Load variability is primarily dependent upon the wind loading on the dish and use of the air-conditioning system. Power can be drawn from the mains or from a 4 kW diesel generator. In either case, backup power sufficient to run the radar for several hours is provided by a 3 kVA uninterruptible power supply with a lead-acid battery pack.

Convective cell observation, Tokoroa, Central North Island, New Zealand

Many precipitation fields, particularly those involving intense convection and instability, exhibit high radar-reflectivity gradients over localised areas and can evolve rapidly in time intervals comparable to radar scan rates. High resolution radar data, like that obtained during MARVEX (Woods *et al.*, 2001), can reveal fine-scale embedded structures, and rapid evolution and advection of rain fields, which is potentially of significant hydrological interest. Such events are poorly sampled with sparse rain gauge networks or long-range operational weather radar networks.

Rain gauges take samples at one point in space, and while they are able to capture changes over time at high resolution, sampling may not be representative of rainfall elsewhere. National radar networks, while sampling a continuous spatial region, make measurements only intermittently, and at long range beam spreading effects can significantly degrade resolution. Both spatial and temporal under-sampling introduce significant uncertainty in areal accumulation estimates. Mobile radar observations can provide much improved (10 sec and 100 m) resolution to observe variable rainfall events over small regions.

During October 2008 and winter 2009, the Trailer Radar was deployed to an elevated position (38° 21' 52.2" S, 175° 43' 11.64" W) near the town of Mangakino and several hydroelectric power stations on the Waikato River in the central North Island of New Zealand to study the implications of sampling scale on radar rainfall rates. The radar was sited to overlook the Waipapa catchment (of extent 10 × 20 km), which feeds into the Waikato River and runs continuously.

The deployment site was chosen for its unobstructed views of the horizon at low scan angles, proximity to the study catchment, and availability of existing power and road infrastructure (the site was adjacent to a dairy shed). However, the choice was still something of a compromise – a hilltop site would have been preferable, but none could be located with an existing power supply. While the chosen site afforded good views, it was found that scan angles of between 4.5° and 6° were required to minimise ground clutter. As multiple scan elevations were employed, the effective scan-rate was 73 seconds. At the short ranges at which the X-band radar operates, this elevation angle constraint is not significant, but at ranges greater than 15 km some beam overshooting of meteorological targets was observed during this study.

During the deployment periods many precipitation weather systems passed over the site, often exhibiting high degrees of heterogeneity. One such case is described to demonstrate the high resolution sampling capabilities of the radar. On 16 October 2008, a cold front advanced from the west. A number of pre-frontal convective cells were detected in the afternoon within the radar's 25 km scan range. The radar images in Figure 2 show a typical example of radar observations of one of the convective cells. This particular storm passed over the nearby town of Tokoroa. The radar slice elevation used to make these plots was 6°, so at 15 km range the reflectivity observation is made at approximately 2.5 km above the ground. The first frames (0 to +5 min) capture the development stage of the storm. The next frames (+10 to +25 min) are characteristic of a mature-stage storm, exhibiting a core with precipitation falling out of an anvil. At around +20 min the core appears to 'stall', propagating backwards in respect to the surrounding advection. In the final frames the storm begins to dissipate.

Other storms observed during this field work also exhibited the characteristic back-building effect, in which new cells form upwind of decaying cores. The back building is presumably due to strong directional shear between upper level and lower level winds, although the radar is not Dopplerised, so no direct measurement of wind speed gradient is available.

Figure 3 is a photograph taken at a time corresponding to the +10 min frame in Figure 2. The area immediately around the radar remained dry, but reports of surface flooding were received from members of the public in Tokoroa. By comparison, one rain gauge, part of the national climate network, was operating in the area at the time, but no precipitation was recorded as the storm did not pass over the gauge.

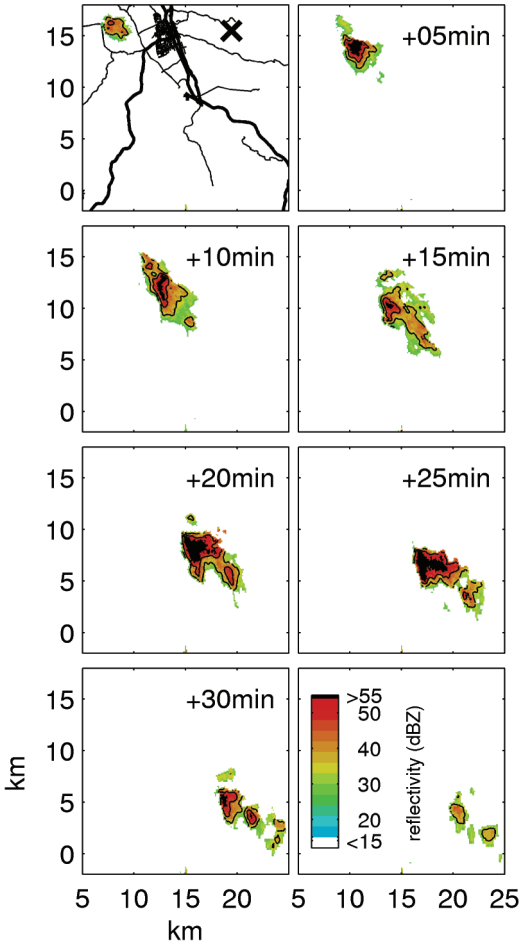

Figure 2 – Time lapse radar reflectivity of a convective cell which formed over Tokoroa on 16 October 2008. Pixels in which reflectivities exceed a threshold of 55 dBZ are limited to 55 dBZ. Contour lines are also drawn at 25, 35, 45 and 55 dBZ. The first frame (+00 min) was observed at 18:03. For context, the first frame shows local roads (solid lines); the confluence of roads around (14,15) is the town of Tokoroa. The radar was located outside the plotted region to the southwest at (0,0). The single permanent rain gauge in the area is indicated (×).

Comparison of X-band radar and rain gauge measurements

The classic metric in radar meteorology is comparison of radar-derived rainfall accumulations and gauge accumulations. When comparing radar and gauge data, it is important to consider possible sources of error. Radar measurements are virtually instantaneous volume samples much larger than the collection area of a gauge, at some distance above the ground. As such, there is no guarantee that a representative sample of rain from the larger volume aloft will make its way into the gauge. The scan interval used in this work, while short compared to intervals typical of national networks, still permits time for unobserved evolution of the rain field between radar sweeps. Such evolution is sampled by accumulating rain gauges, which are unable to make instantaneous measurements for comparison to radars, possibly leading to discrepancies in accumulation. Assumptions about the drop-size distribution made in order to convert reflectivity to rainfall rate can result in significant uncertainty in radar-derived rainfall rate retrievals, if the hydrometeor type differs significantly from the climatological average. In addition, as the Z-R relationship is a power law, beam spreading and incomplete beam filling associated with large sampling volumes compared to the scale of heterogeneity in the rain field has the effect of smoothing out the rainfall intensity, as well as adding an overall positive bias to the rainfall rate (Randeu and Schonhuber, 2000). All these sources of error should be reduced with an X-band system at short range compared to national C-band networks at longer range. By scanning as close to the ground as possible, and at a high spatial and temporal resolution, representivity and sampling errors associated with finite sample volume and scan time will be reduced, potentially improving comparison with point gauge measurements.

Figure 3 – Photograph taken from the radar site of the storm over Tokoroa on 16 October 2008 (reflectivity data in Figure 2).

A full comparison of the magnitude of these uncertainties between X-band and C-band radars is beyond the scope of this paper, however it is instructive to review the limitations of both the mobile X-band and more remote fixed C-band radars before continuing with a gauge comparison. Coincident observations of rain from a frontal system passing over the study site from both the X-band and two C-band radars (from the New Zealand National Network located at New Plymouth and Warkworth) are shown in Figure 4. The higher axial spatial resolution of the nearer X-band radar is apparent, particularly for the narrow rain band in the western side of the images – the elongation of pixels in the axial direction is distinct in the two scans from the national radars. The variation in axial resolution is dependent on the different locations and beam widths of the X-band and C-band radars. In fact, the more distant C-band radars have about twice the angular resolution of the closer X-band radar, but the resolution over the study site is worse because they are much more than two times further away.

Evident in the X-band scan are high-intensity cores with horizontal extents of a few hundred metres, but these are absent in the equivalent C-band images. Beam spreading effects will tend to smooth out and reduce the mean reflectivity of a non-uniformly filled sampled volume. This is an important consideration for hydrological applications, as the Z-R relationship responds strongly to high reflectivity, so that smoothing with a slight negative bias causes a strong reduction in retrieved rainfall rate.

The variation of reflectivity with height suggests that radar observations made closer to the ground will be more representative of surface rainfall rate. Figure 5 (top) shows a vertical slice through the same rain band shown in the west in Figure 4. The precipitation structure extends to some 4 km altitude, with some variability over its height, and it exhibits a decrease in reflectivity above about 3 km. In this case no bright band is apparent and the rain is probably only convective. The beam scanning volume of the nearby X-band radar is indicated on the diagram, intersecting the cell around 800 m above the ground. The volume of the New Plymouth radar beam at the range of this cell is by comparison wide, illuminating a cross-section from 2 to 5 km altitude. At long range, the Earth's curvature and beam spreading effects mean that, even with a low scan elevation, the C-band radar beam is only partially incident on the convective cell, so the volume average cannot

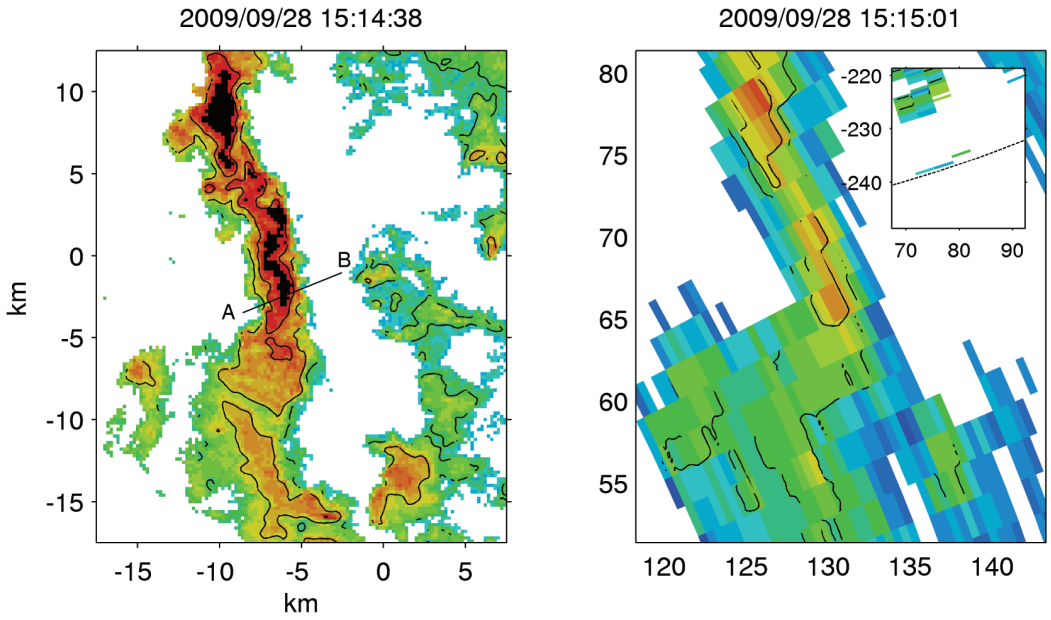

Figure 4 – Lowest available radar scans of the same area and time above the field site from the UoAAPG X-band radar (left) and the NZ MetService C-band radars located at New Plymouth (right) and North of Auckland (right inset). For the Auckland radar, the lower half of the domain is outside the maximum range of the radar. The reflectivity scale and contour intervals are the same as for Figure 2 and the axis scale indicates the distance of the observations from the respective radars ((0,0) is redefined as the location of the observing radar in each plot). A vertical cross-section along A-B is shown in Figure 5.

be representative of reflectivity near the surface. By comparison, the X-band radar scan at short ranges is low enough to slice through the cell and obtain a sample representative of the surface precipitation. But site limitations (discussed earlier) led to the use of a high scan angle, so the X-band beam climbs quickly with range and would begin to overshoot a similar convective target at just a 20 km range. For comparison, Figure 5 (bottom panel) shows a vertical profile during some largely stratiform cool precipitation earlier in the project. A bright band, associated with melting snow, is apparent at just below 2 km altitude. In this case, the X-band radar scans could only be considered representative of the surface reflectivity out to a little over a 10 km range.

In the radar scans shown in Figure 4, it is not possible to separate differences in reflectivity measurements between radars due to sampling resolution limitations from the variability in reflectivity with altitude. An estimate of the resolution-dependent error can however be obtained (Fabry *et al.*, 1994) by degrading the X-band image's resolution in space in a way physically analogous to averaging over the rain field and then comparing it to the original non-degraded field. This spatial error analysis technique is explored in some detail for the same 3 month dataset elsewhere (Shucksmith, Sutherland-Stacey and Austin, 2011) where an average error of about 10% in 10 minute rainfall accumulations is introduced by degrading the spatial resolution from 200 m to 500 m and 20% error when degrading to 1000 m.

The other major source of scale representation error in typical national radar observa-

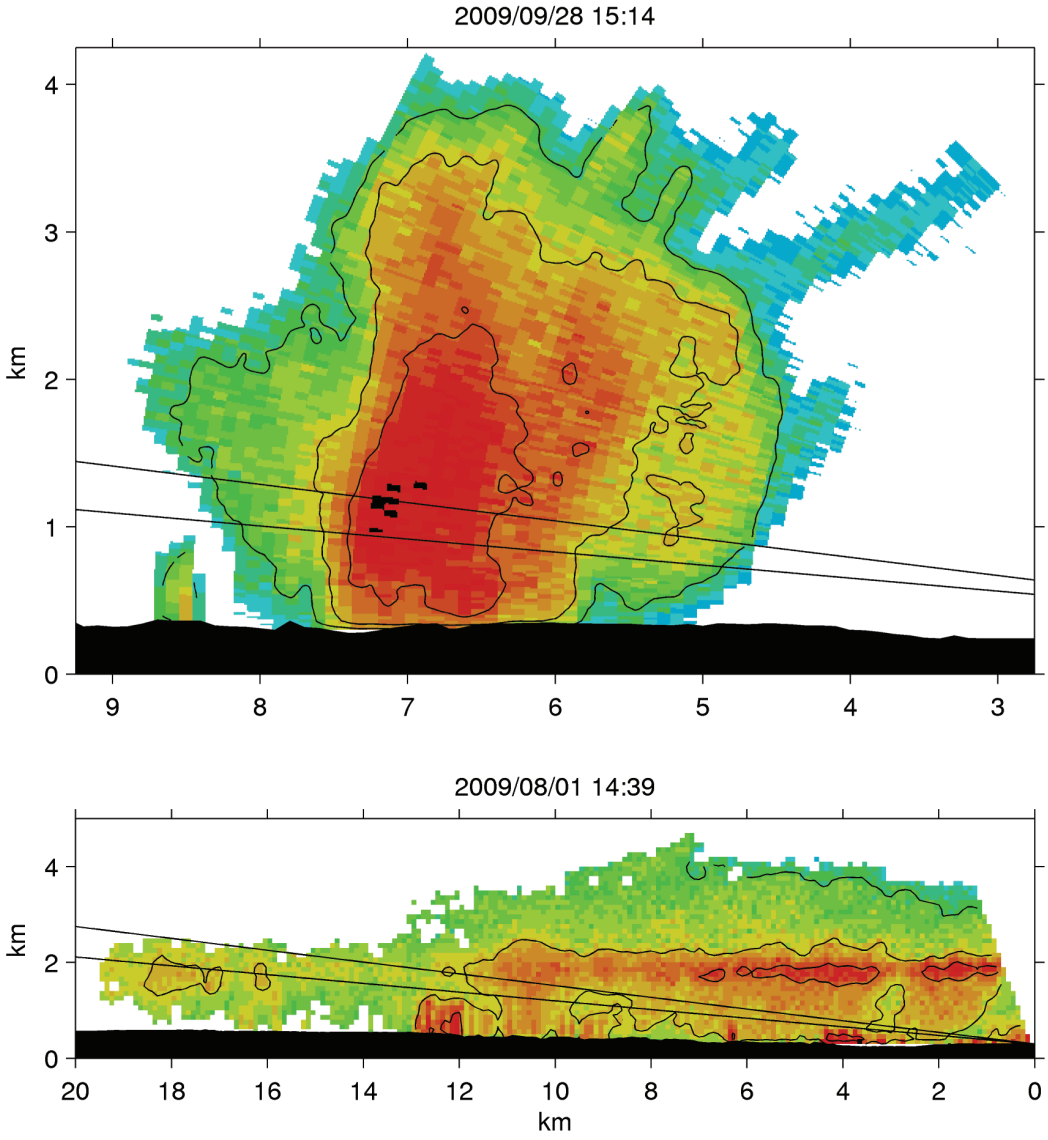

Figure 5 – *Top:* Vertical reflectivity cross-section along the line A-B (shown in Figure 4). The beam width of the 6° elevation X-band radar scan is indicated. *Bottom:* Vertical reflectivity cross-section taken during the event depicted in Figure 7 (right) with the X-band beam width indicated.

tions is the period between scans (7.5 minutes for the New Zealand network). An estimate of this temporal representation error can be obtained by comparing X-band accumulation maps generated from a full complement of (relatively) frequent scans to maps generated from only a subset of the same scans. In Figure 6, 1-hour accumulations generated from either a full set of 49 X-band scans (1 and 2), or a subset of only 8 scans

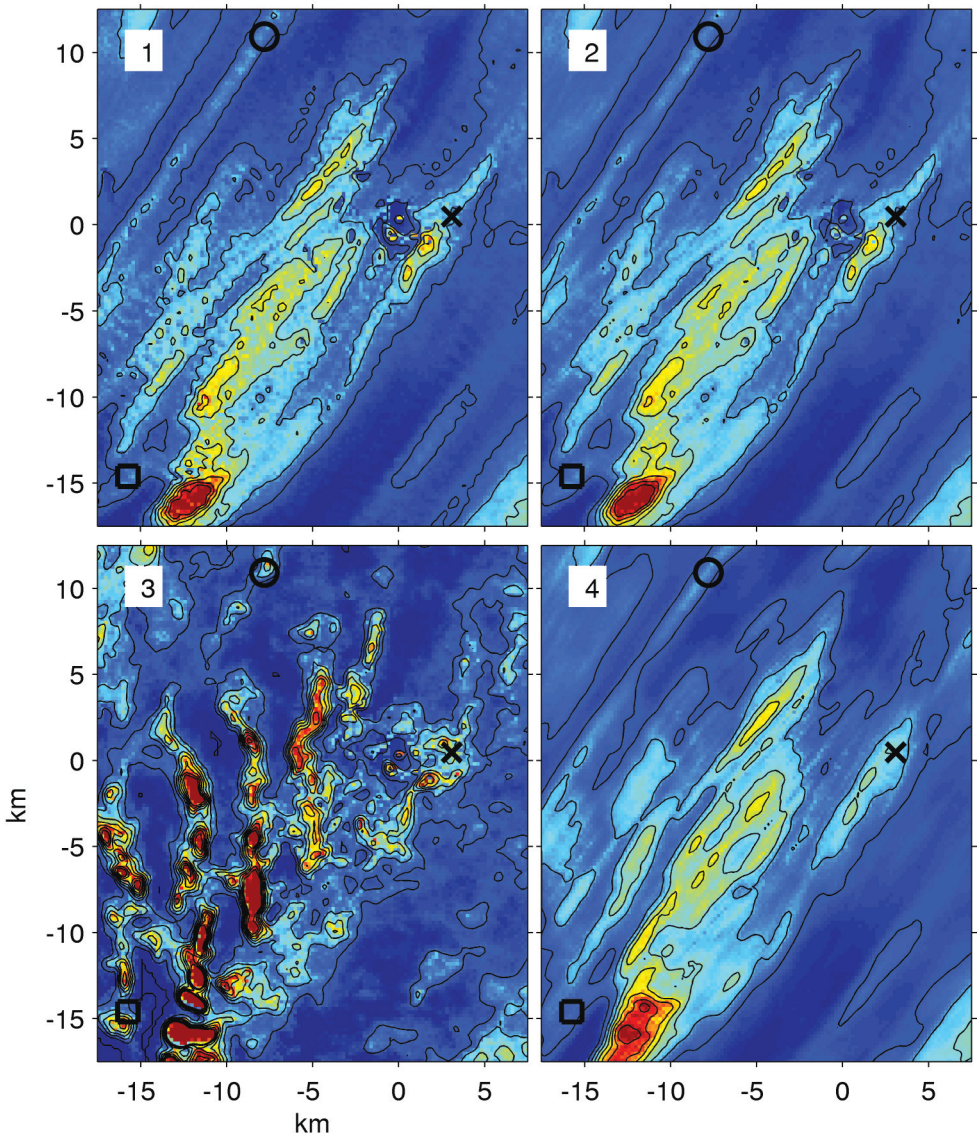

Figure 6 – 60-minute X-band radar rainfall accumulations for the period ending 2009/09/28 at 15:30. The four accumulations are generated using two different scan frequencies and show the effect of ignoring or attempting to account for the unobserved advection of the rain field between scans.

1) 49 scans (73 second sampling interval), static accumulation scheme.
2) Same as 1 but with an advection accumulation scheme.
3) 8 scans (7.5 minute sampling interval). Static accumulation scheme.
4) Same as 3 but with an advection accumulation scheme.

The location of the rain gauges compared in Figure 7 are shown (×, □ and ○). Contour lines are drawn every 2 mm.

(3 and 4) is presented. The accumulations are generated using one of two algorithms. In the first accumulation scheme (1 and 3) no effort is made to account for the advection of the rain field between measurements and the accumulation is generated by applying the classic Marshal-Palmer (1948) Z-R relationship ($Z = 200R^{1.6}$) to each reflectivity image, multiplying by the time interval between scans and finally summing over all scans. In the second scheme (2 and 4), an echo motion vector is diagnosed by finding the maximum cross-correlation between sequential reflectivity images and then the diagnosed rainfall from each scan is smoothed in the direction of motion before accumulation. From the simple accumulation scheme, it is apparent that the higher scan frequency (1) generates a more physically realistic accumulation than the lower scan frequency (3). Applying the advection accumulation scheme on the high scan rate dataset (2) has little effect on the hourly accumulation. This is because, at the approximately 200 m spatial resolution of the X-band measurement, the advection in the 73 seconds between scans is not much more than the pixel size, with only a subtle banding or ripple structure apparent in (1) compared to the distinct bands in (3). However, when the advection scheme is applied to the low scan rate subset (4), an accumulation map similar in appearance to (1) and (2) is generated. The remaining differences between (4) and (1 and 2) can then be attributed to the unsampled evolution of the rain field, for example the decay or growth of convective cells, between scans. The error introduced by reduced sampling frequency is also explored for the whole three-month dataset by Shucksmith *et al.* (2011), in which an average error in 10 minute accumulations (generated with the advection interpolation scheme) of about 20% is introduced by degrading from a 73 second to a 7.5 minute sampling rate.

Despite the uncertainties introduced by poorer spatial and temporal resolution and beam overshooting and spreading, the distant C-band radars do qualitatively detect rain in similar locations to the X-band radar. Since the work reported here has been completed, a new C-band radar system has been made operational in the Mamaku Plateau, so that the Waipapa site is now better covered by the national radar network at a range suitable for quantitative radar estimates of precipitation.

To test the retrieval of rainfall rate from the X-band Trailer Radar reflectivity measurements, data from 12 rain gauges within 25 km of the radar site were collated and compared to a radar-derived accumulation estimate. Seven (Davis) tipping-bucket rain gauges were distributed around the area on local farms specifically for this work. The gauges record the time of individual 0.254 mm tips. To help overcome quantisation errors associated with the discrete tips (Habib *et al.*, 2001) the gauge data was accumulated into 15 minute time bins. Further rain gauge data was obtained from five permanent gauges operated by the National Institute of Water and Atmospheric Research (NIWA) as 15 minute accumulations.

Radar-derived accumulations were generated for the (X-band) pixels directly above each gauge by first treating successive radar reflectivity measurements using a Z-R relationship ($Z = 200R^{1.6}$) and then summing with a weighting proportional to the time until the next image. This is equivalent to the first accumulation scheme described earlier, in that it does not allow for advection between scans. The simple scheme is used as it is computationally cheap, and at the high scan rates used in this work there is little difference in accumulations when applying the advection accumulation scheme.

Gauge correction methods, whereby tuning functions are found which minimise the discrepancy between radar and in-situ point rain gauge observations, are widely used in operational work. For this study, a range-dependent bias was determined by

accumulating over the total experimental period and then binning the accumulations as a function of range from the radar. By assuming that the actual accumulation over the region should not be related to the distance from the radar, a range-dependent correction factor is thus derived to correct (increase) the retrieved rainfall rate at longer ranges. The data is corrected only once with this range-dependent (but time-independent) variable.

Comparisons between rain gauge measurements and radar-derived rainfall rates for three different gauges at distances of 3.1, 13.4 and 21.5 km from the radar are presented in Figure 7. For the nearest of the three plotted gauges (Fig. 7, top), the charts show good agreement between radar and gauge rainfall rates in both instantaneous intensity and total accumulation. This is expected – for gauges sited close to the radar, the radar beam samples a small volume not far above the gauge which minimises, but does not eliminate, representation errors. The left panels in Figure 7 span a period from which the examples presented in Figures 4-6 are derived. A significant disagreement between the gauge and radar-derived rainfall rate can be observed in the left 3.1 km panel at about 15:30, when the intense rain band crosses the gauge location. It is apparent from the accumulation diagram (Fig. 6) that there is a sharp spatial gradient in rainfall in the vicinity of the gauge (indicated with an ×). It is possible that in this case there was some location error between the gauge and radar observation, for example wind advection of precipitation can introduce spatial representation error between the gauge and radar pixel. Another possible explanation is an unsampled localised brief intensification in precipitation between scans that could have resulted in a large accumulation being recorded by the gauge compared to the coincident radar pixel. In contrast, the top right panel does not exhibit any large instantaneous disagreement between instantaneous radar and accumulated gauge measurements. The meteorological situation during the right period was widespread stratiform rain (e.g., Fig. 5, bottom), which typically is less variable than convective rain. Reduced spatial and temporal variability should mean that the representativity error between radar pixels and sub-pixel gauge measurements is correspondingly reduced.

The middle and bottom set of panels in Figure 7 cover the same time periods of predominantly convective (left) and stratiform (right) rain as the short-range radar-gauge comparison (top) but are for gauges located considerably further from the radar. The agreement in instantaneous rainfall rate and total accumulation for both the gauges at 14.4 and 21.5 km and the corresponding radar pixels is generally poorer than at shorter range, however the structure of the rain event is still resolved for both the stratiform and convective rain. The 14.4 km gauge-radar difference in accumulation for the stratiform case is almost 30 mm. The radar over-estimation is likely due to the radar beam intersecting the bright band at around a 14 km range during this event Fig. 5, bottom). This enhanced reflectivity signal (the origins of which are discussed earlier) results in positive bias in the derived rainfall rate. Above the gauge at 21.5 km range the beam also intersects the bright band and the frozen layer above, however less rain fell during this period in the south-west where the gauge is located, so the disagreement is not so pronounced in terms of absolute error. In contrast to the poorer performance at range during stratiform events, the agreement in gauge-radar total accumulations are better for the convective rain (Fig. 7, left panels). This could be attributed to a large extent to measurements of deeper convective structures made aloft more fully representing rainfall at the ground.

These qualitative examples serve as a reminder of the difficulties in comparing

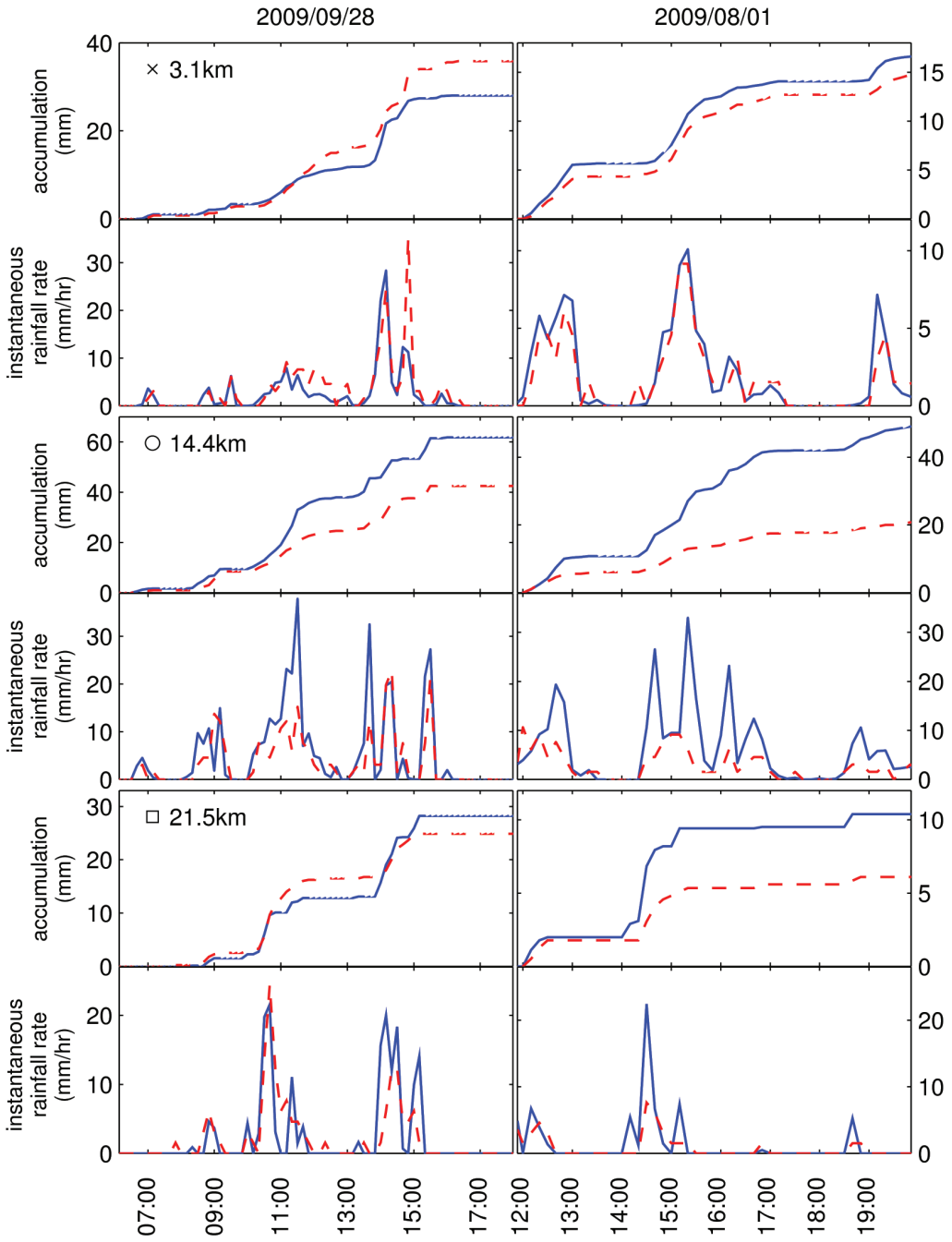

Figure 7 – Comparison of accumulation (top panels) and rainfall rate (bottom panels) derived from X-band radar (solid) and gauge measurements (dashed) for two different time periods and three different gauges. The range of each gauge and symbols corresponding to Figure 6 and Table 1 are in the top left corner for each set of four plots

gauge point measurements with radar observations. Although over an area the radar may instantaneously image the rainfall from fine-scale structure some hundreds of metres above the ground well, it is still difficult to exactly match a particular part of that image to a gauge measurement that is by comparison of infinitesimal extent, displaced in the vertical and a continuous record rather and an instantaneous sample.

At shorter ranges the errors associated with the imprecise correction for attenuation at X-band wavelengths and sensitivity effects are minimal. At longer range the opposite is true, and the X-band radar behaves more like a C-band radar at considerably longer ranges (in addition to suffering from beam overshooting and spreading effects) and agreement between the X-band radar data and gauge measurements) is qualitatively much poorer.

To rigorously compare the X-band radar rainfall retrievals over the whole 25 km scan range with rain gauge measurements, various standard statistical measures – mean absolute error (MAE), root mean square error (RMSE) and the R^2 statistic – were calculated for 1-hour accumulation periods. The MAE is defined as

$$\mathrm{MAE} = \frac{\sum_{i=1}^{N} |G_i - R_i|}{N},$$

where G and R are the gauge 1-hour rainfall accumulations and N is the total number of 1-hour periods containing rainfall. Likewise the RMSE is defined as

$$\mathrm{RMSE} = \sqrt{\frac{\sum_{i=1}^{N} (G_i - R_i)^2}{N}}$$

The R^2 statistic is calculated in the usual way for each hourly period in which the gauge reported a rainfall rate in excess of 1 mm/hr. The first and second moments (the mean and standard deviation) of the R^2 statistics were determined for each gauge.

The resulting statistics for the whole data set collected over the three-month field campaign are presented in Table 1.

Unsurprisingly, the quantitative agreement between radar retrieval and gauge is range dependent, with all statistics indicating better agreement at shorter ranges. Beyond about a 20 km range it is apparent that the radar-derived accumulation compares very poorly with gauge measurements, and representation errors due to beam overshooting of meteorological targets, beam spreading, poor representativity of reflectivity aloft, and the limited X-band radar power are likely to have been significant.

Table 1 – Mean absolute error (MAE), root mean square error (RMSE) and the R2 statistic for gauge vs. radar-retrieval 1 hour accumulations (sorted by range). Gauges referred to in Figures 6 and 7 are indicated with their corresponding symbols in the range column.

Range (km)	MAE (mm)	RMSE (mm)	R^2 Mean (stdev)
3.1×	0.54	1.5	0.77(0.19)
5.6	0.50	1.0	0.72(0.24)
7.1	0.57	1.0	0.68(0.26)
13.4○	0.92	1.7	0.52(0.25)
18.0	0.81	1.5	0.56(0.29)
18.4	1.02	1.8	0.53(0.26)
20.0	0.96	1.8	0.53(0.27)
21.5□	0.93	1.6	0.53(0.28)
23.4	1.5	2.6	0.42(0.25)
24.5	1.8	3.0	0.30(0.24)
24.8	1.3	2.5	0.28(0.22)
24.8	1.5	3.1	0.47(0.30)

Comparative statistics from similar gauge studies involving C-band radar networks with lower resolution spatial and temporal characteristics include gauge-radar RMS errors of 3.1-3.9 mm/hr (Chumchean, Sharma and Seed, 2006), 2.2-7.0 mm/hr (Ryzhkov *et al.*, 2005) and 0.6-1.0 mm/hr (Vignal and Krajewski, 2001). A similar experiment using a more powerful X-band radar resulted in RMSEs of 0.5-3.0 mm/hr (Gerstner and Heinemann, 2008). Gray and Austin (1993) report R^2 values of 0.25-0.63 for comparisons between gauge and radar retrievals in Otaki, New Zealand on a per-event basis. The results reported in this work are for much shorter ranges and higher spatial and temporal sampling rates, and the better RMSEs and R^2 statistics for the three nearest gauges can probably be attributed primarily to improved sampling scale. The poorer results for this study than for other works at longer range is probably related to the comparatively low power of the transmitter, reduced spatial resolution and overshooting due to the necessity of using a relatively high scan angle.

Considerations of scale-related errors for hydrological modelling applications

While rain gauges measure point accumulations with some certainty, spatial variability of the rain fields makes it particularly difficult to use a (usually irregular) distribution of gauges to determine the rainfall rate at points that are not near a gauge. An even more complicated task is to estimate total catchment accumulations from a small number of gauges. By considering the radar mean decorrelation length scale (the horizontal displacement at which the cross correlation of a radar image reduces to a factor of e^{-1}), an estimate of the gauge density that would be required to resolve the field can be made. For the data collected in this study, the histogram of length scale for individual radar images takes the form of an exponential decay function with 90% of precipitating images having a decorrelation length of less than 6 km. By comparison, the Waipapa catchment (of some 10 km × 20 km extent) contains only one rain gauge.

The implications of the gauge spatial under-sampling problem can be demonstrated by considering the difference in total catchment accumulation as measured by radar compared to a point measurement. In Figure 8, the average catchment radar-retrieved accumulation is compared to both gauge and radar-retrieved point measurements for a rain event on 23-24 October 2008. The radar and gauge point measurements are in good agreement, but the catchment accumulation as determined by the radar was twice the amount that would be estimated by assuming the rain gauge measurement at the catchment outlet is representative of the catchment as a whole. The origin of the discrepancy can be immediately identified by reviewing the radar images of the event

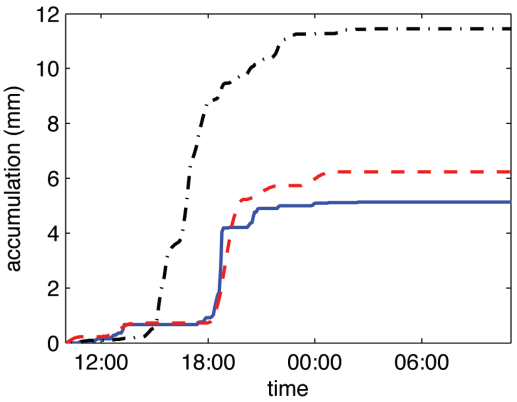

Figure 8 – Accumulations for a rain event on 23-24 October 2008 generated from a rain gauge located at the Waipapa catchment outlet (dashed), the X-band radar pixel corresponding to the gauge location (solid) and the average catchment accumulation generated from radar images (dot-dashed).

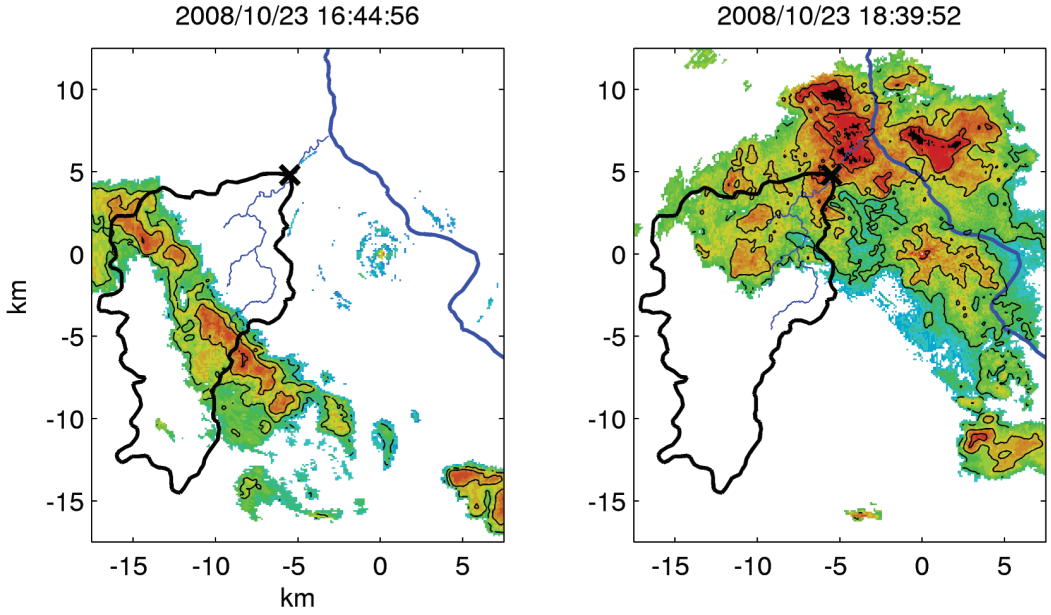

Figure 9 – Selected radar reflectivity images corresponding to the rainfall retrievals in Figure 8 (the reflectivity scale is the same as for Figure 2). The X-band radar is located at (0,0) and the location of rain gauge run by NIWA is indicated (×). The Waipapa catchment is indicated with a solid closed loop. The Waikato river flows across the north-east quadrant of the image (solid line) and major tributaries in the Waipapa catchment are also indicated (lighter lines).

(Fig. 9). A number of convective cells pass through the centre of the catchment but not over the gauge site, meaning much more rain fell into the catchment than could be sampled by the gauge. For other rain events the opposite was true, with cells passing over the gauge but not the western reaches of the catchment.

Such rain gauge measurement representation errors are often largely ignored in workaday applications of hydrological modelling. To some extent this is not unsafe practice for large catchments, where response times on the order of days or weeks mean only long length and timescale processes are significant. For smaller catchments, however, just one convective cell could deliver hydrologically significant precipitation, particularly in steep terrain where time to concentration is short. If a well calibrated model for this small catchment was fed with either the radar or rain gauge data, the behaviour of the model would be quite different. The radar-fed model would receive water input ahead of the gauge estimate and in larger volumes, so would 'know' more about reality and should therefore make 'better' predictions about the future state of the catchment. Using only low sparse gauge data, the catchment might appear to behave erratically, if the representation uncertainty is not properly considered.

Discussion and conclusions

It is evident that convective precipitation systems may show microscale structure (<1 km) and rapid evolution (<1 minute). Such small-scale structures are often left unresolved by most operational radar systems or gauge networks. Portable X-band radar

systems, such as the one recently developed by UoAAPG, provide improved spatial and temporal resolution to observe such events near regions of hydrological interest for specific studies, at the expense of coverage area.

The examples presented here exhibited fine-scale structure and rapid evolution which at times were not as well sampled by gauge networks. The traditional gauge-radar comparison shows some improvement when using high resolution X-band radars, probably because of reduction in sampling resolution and intermittency errors. However, there is no reason to assume that such errors are totally eliminated from the X-band radar data at the resolutions and scan rates used in this work – in the case of the discontinuities visible in accumulation fields there is good evidence that they are not. Even higher resolutions would no doubt be of scientific and operational interest.

Of particular significance, however, are the implications of spatial and temporal sampling errors to downstream use of catchment-scale accumulation estimates. In this study catchment accumulations derived from point measurements were at times in significant disagreement with an areal measurement generated from radar data (in these cases the major source of error was attributed to the poor spatial sampling characteristics of rain gauges). The implications for hydrological modelling of such large errors in small-scale catchment accumulations are important – if a model is tuned based on erroneous input accumulation to match output river stage, then catchment parameters could be poorly calibrated, reducing model utility for prediction of future river flow. Without spatially resolved observations, the validity of using point gauge measurements (regardless of the interpolation scheme) to estimate total catchment accumulation is tenuous, as it is not possible to be sure that the point measurements are truly representative.

Acknowledgements

The Trailer Radar was constructed by the Physics Department Mechanical Workshop staff and Physics Department Electronics Technicians: special thanks are extended to Steve Warrington, Matthew Hogg, Kevin George, Murray Hollis and Ian Guthrie. A significant fraction of the radar control code was written by former student Andrew Peace. Wrights Technologies Limited and VisSim AS assisted with modification of the radar transceiver. C-band radar data from the New Zealand National Radar Network has been kindly provided by the NZ MetService.

References

Atlas, D.; Banks, H.C. 1951: The Interpretation Of Microwave Reflections From Rainfall. *Journal of Meteorology 8*: 271-282.

Austin, G.L. 1974: Pulse-Compression Systems for use with Meterological Radars. *Radio Science 9*: 29-33.

Austin, P.M.; Bemis, A.C. 1950: A quantitative study of the bright band in radar precipitation echoes. *Journal of Meteorology 7*: 145-151.

Biggerstaff, M.I.; Wicker, L.J.; Guynes, J.; Ziegler, C.; Straka, J.M.; Rasmussen, E.N.; Doggett, A.; Carey, L.D.; Schroeder, J.L.; Weiss, C. 2005: The shared mobile atmospheric research and teaching radar - A collaboration to enhance research and teaching. *Bulletin of the American Meteorological Society 86*: 1263-1274.

Bitew, M.M.; Gebremichael, M. 2010: Spatial variability of daily summer rainfall at a local-scale in a mountainous terrain and humid tropical region. *Atmospheric Research 98*: 347-352.

Bluestein, H.B.; French, M.M.; Tanamachi, R.L.; Frasier, S.; Hardwick, K.; Junyent, F.; Pazmany, A.L. 2007: Close-range observations of tornadoes in supercells made with a dual-polarization, X-band, mobile Doppler radar. *Monthly Weather Review 135*: 1522-1543.

Changnon, S.A. 2002: Hydroclimatic differences in precipitation measured by two dense rain gauge networks. *Journal of Hydrometeorology 3*: 66-79.

Cheze, J.L. 2002: The Aramis weather radar network and its qualitative and quantitative uses. *Houille Blanche-Revue Internationale De L Eau*: 37-41.

Cho, J.; Bosch, D.; Lowrance, R.; Strickland, T.; Vellidis, G. 2009: Effect of spatial distribution of rainfall on temporal and spatial uncertainty of SWAT output. *Transactions of the ASABE 52*: 1545-1555.

Chumchean, S.; Sharma, A.; Seed, A. 2006: An integrated approach to error correction for real-time radar-rainfall estimation. *Journal of Atmospheric and Oceanic Technology 23*: 67-79.

Collier, C.; Blyth, A.; Hobby, M.; McCarroll, C.; McGonigal, J.; McLaughlin, D.; Nolan, M. 2011: Adaptive phased array radar technology for urban hydrological forecasting. In *Weather Radar and Hydrology*. Exeter, United Kingdom.

Cooper, M.R.; Fernando, D.A.K. 2009: *The effect of the raingauge distribution on stormwater models*. Nedlands, University of Western Australia.

Crouch, J. 2003: Using Radar to Diagnose Weather Systems. *Tephra 20*: 46-48.

Crum, T.D.; Alberty, R.L. 1993: The WSR-88D and the WSR-88D operational support facility. *Bulletin of the American Meteorological Society 74*: 1669-1687.

Cunningham, R.M. 1947: A different explanation of the bright line. *Journal of Meteorology* 4: 163-163.

Delrieu, G.; Braud, I.; Berne, A.; Borga, M.; Boudevillain, B.; Fabry, F.; Freer, J.; Gaume, E.; Nakakita, E.; Seed, A.; Tabary, P.; Uijlenhoet, R. 2009: Weather radar and hydrology - Preface. *Advances in Water Resources 32*: 969-974.

Doviak, R.J.; Zrnic, D.S. 1993: *Doppler radar and weather observations*. San Diego; London: Academic Press.

Dozio, L.; Mantegazza, P. 2003: Real time distributed control systems using RTAI. *In* Puschner, P.; Nakajima, T.; Ghafoor, A. (*eds.*) *6th IEEE International Symposium on Object-Oriented Real-Time Distributed Computing*. Hakodate, Hokkaido, Japan, 14-16 May 2003: 11-18.

Duncan, M.R.; Austin, B.; Fabry, F.; Austin, G.L. 1993: The effect of gauge sampling density on the accuracy of streamflow prediction for rural catchments. *Journal of Hydrology 142*: 445-476.

Fabry, F.; Bellon, A.; Duncan, M.R.; Austin, G.L. 1994: High resolution rainfall measurements by radar for very small basins: the sampling problem reexamined. *Journal of Hydrology 161*: 415-428.

Fabry, F.; Zawadzki, T. 1995: Long-term radar observations of the melting layer of precipitation and their interpretation. *Journal of the Atmospheric Sciences 52*: 838-851.

Fiener, P.; Auerswald, K. 2009: Spatial variability of rainfall on a sub-kilometre scale. *Earth Surface Processes and Landforms 34*: 848-859.

Gerstner, E.M.; Heinemann, G. 2008: Real-time areal precipitation determination from radar by means of statistical objective analysis. *Journal of Hydrology 352*: 296-308.

Gray, W.R.; Austin, G.L. 1993: Estimation by radar for the Otaki catchment: The OPERA pilot study. *Journal of Hydrology (New Zealand) 31*: 91-110.

Gray, W.R.; Seed, A.W. 2000: The characterisation of orographic rainfall. *Meteorological Applications 7*: 105-119.

Gray, W.R.; Uddstrom, M.J.; Larsen, H.R. 2002: Radar surface rainfall estimates using a typical shape function approach to correct for the variations in the vertical profile of reflectivity. *International Journal of Remote Sensing 23*: 2489-2504.

Habib, E.; Krajewski, W.F.; Kruger, A. 2001: Sampling errors of tipping-bucket rain gauge measurements. *Journal of Hydrologic Engineering 6*: 159-166.

Heinselman, P.L.; Torres, S.M. 2011: High-Temporal-Resolution Capabilities of the National Weather Radar Testbed Phased-Array Radar. *Journal of Applied Meteorology and Climatology 50*: 579-593.

Henderson, R.D.; Thompson, S.M. 1999: Extreme Rainfalls in the Southern Alps of New Zealand. *Journal of Hydrology (New Zealand) 38*: 309-330.

Krajewski, W.F.; Lakshmi, V.; Georgakakos, K.P.; Jain, S.C. 1991: A Monte-Carlo study of rainfall sampling effect on a distributed catchment model. *Water Resources Research 27*: 119-128.

Larsen, H.R.; Gray, W.R. 2003: Assessment of a radar-based nowcasting model for the Auckland region. *Journal of Hydrology (NZ) 42*: 101-112.

Mann, N.K. 1998: X-Band Radar Measurements of Volcanic Ash Plumes: Ruapehu Eruption 1996. MSc Thesis, University of Auckland.

Marshall, J.S.; Palmer, W.M. 1948: The Distribution Of Raindrops With Size. *Journal of Meteorology 5*: 165-166.

McMillan, H.; Jackson, B.; Clark, M.; Kavetski, D.; Woods, R. 2011: Rainfall uncertainty in hydrological modelling: An evaluation of multiplicative error models. *Journal of Hydrology 400*: 83-94.

Nicol, J.C.; Austin, G.L. 2003: Attenuation correction constraint for single-polarisation weather radar. *Meteorological Applications 10*: 345-354.

Pedersen, L.; Jensen, N.E.; Christensen, L.E.; Madsen, H. 2010: Quantification of the spatial variability of rainfall based on a dense network of rain gauges. *Atmospheric Research 95*: 441-454.

Prat, O.P.; Barros, A.P. 2010: Ground observations to characterize the spatial gradients and vertical structure of orographic precipitation - Experiments in the inner region of the Great Smoky Mountains. *Journal of Hydrology 391*: 143-158.

Purdy, J.C.; Austin, G.L.; Seed, A.W.; Cluckie, I.D. 2005: Radar evidence of orographic enhancement due to the seeder feeder mechanism. *Meteorological Applications 12*: 199-206.

Randeu, W.L.; Schonhuber, M. 2000: Rainfall overestimates induced by radar area averaging. *Physics and Chemistry of the Earth, Part B: Hydrology, Oceans and Atmosphere 25*: 965-969.

Reichel, F.; Verworn, H.R.; Kramer, S.; Cluckie, I.; Rico-Ramirez, M.A. 2009; Radar-based flood forecasting for river catchments. *Proceedings of the Institution of Civil Engineers-Water Management 162*: 159-168.

Ryde, J.W. 1946: The attenuation and radar echoes produced at centimetre wave-lengths by various meteorological phenomena. In *Meteorological factors in radio-wave propagation*. The Royal Institution, London: The Physical Society.

Ryzhkov, A.V.; Schuur, T.J.; Burgess, D.W.; Heinselman, P.L.; Giangrande, S.E.; Zrnic, D.S. 2005: The joint polarization experiment - Polarimetric rainfall measurements and hydrometeor classification. *Bulletin of the American Meteorological Society 86*: 809-824.

Shucksmith, P.E.; Sutherland-Stacey, L.; Austin, G.L. 2011: The spatial and temporal sampling errors inherent in low resolution radar estimates of rainfall. *Meteorological Applications*.

Sutherland-Stacey, L.; Shucksmith, P.; Austin, G. 2010: High Resolution Observation of a Small Tornado, Ardmore, New Zealand. *Weather and Climate 30*: 46-53.

van de Beek, C.Z.; Leijnse, H.; Stricker, J.N.M.; Uijlenhoet, R.; Russchenberg, H.W.J. 2010: Performance of high-resolution X-band radar for rainfall measurement in The Netherlands. *Hydrology and Earth System Sciences 14*: 205-221.

Vignal, B.; Krajewski, W.F. 2001: Large-sample evaluation of two methods to correct range-dependent error for WSR-88D rainfall estimates. *Journal of Hydrometeorology 2*: 490-504.

Villarini, G.; Krajewski, W.F. 2010: Review of the different sources of uncertainty in single polarization radar-based estimates of rainfall. *Surveys in Geophysics* 31: 107-129.

Villarini, G.; Mandapaka, P.V.; Krajewski, W.F.; Moore, R.J. 2008: Rainfall and sampling uncertainties: A rain gauge perspective. *Journal of Geophysical Research - Atmospheres 113*, D11102, doi:10.1029/2007JD009214.

Woods, R.A.; Grayson, R.B.; Western, A.W.; Duncan, M.; Wilson, D.J.; Young, R.I.; Ibbitt, R.; Henderson, R.; McMahon, T.A. 2001: Experimental Design and Initial Results From the Mahurangi River Variability Experiment: MARVEX. Pp. 201-213 in Lakshmi, V.; Albertson, J.; Schaake, J. (*eds.*) *Water science and application*, Washington, DC, American Geophysical Union.

Wurman, J.; Straka, J.; Rasmussen, E.; Randall, M.; Zahrai, A. 1997: Design and deployment of a portable, pencil-beam, pulsed, 3-cm Doppler radar. *Journal of Atmospheric and Oceanic Technology 14*: 1502-1512.

Xiao, Q.N.; Kuo, Y.H.; Sun, J.Z.; Lee, W.C.; Barker, D.M.; Lim, E. 2007: An approach of radar reflectivity data assimilation and its assessment with the inland QPF of Typhoon Rusa (2002) at landfall. *Journal of Applied Meteorology and Climatology 46*: 14-22.

Manuscript received 23 February 2011; accepted for publication 10 July 2011